Identification of Cellular Signal Measurements Using Extreme Learning Machine

Esraa A. Makled, Ibrahim Al-Nahhal, *Senior Member, IEEE*, Octavia A. Dobre, *Fellow, IEEE*, Oktay Üreten, and Hyundong Shin, *Fellow, IEEE*

***Abstract*—Intelligent radios play a pivotal role in optimizing communication resources for both commercial and military applications. Automatic signal identification (ASI) serves as a crucial component for intelligent radios, with likelihood-based and feature-based ASI algorithms being conventional approaches. Recent studies have explored the integration of machine learning (ML) algorithms for ASI, revealing their enhanced resilience to channel distortions compared to traditional methods. This article proposes the application of an extreme learning machine (ELM), a type of the ML algorithm, for the identification of cellular signals based on over-the-air measurements of power spectral density (PSD). The proposed ELM undergoes evaluation using two distinct datasets of PSDs to assess identification accuracy, with the first dataset utilized for hyperparameter optimization and the second unseen dataset employed to evaluate robustness and generality. The experimental results showcase improved performance in both accuracy and training complexity compared to recent work in the literature.**

***Index Terms*—Extreme learning machine, over-the-air data, real cellular PSD measurements, signal identification.**

I. Introduction

THE RISE in the number of wireless devices elevated the demand on the scarce radio spectrum. This urged the need to utilize the spectrum efficiently. Intelligent radios efficiently use communication resources for commercial and military purposes [1]. Applications of intelligent radios include spectrum allocation, interference mitigation, and intelligent signals [1], [2], [3]. Automatic signal identification (ASI) plays a pivotal role in intelligent radios [2], [3]. The classical ASI algorithms are likelihood-based and feature-based, as extensively discussed in the literature, such as [1], [4], [5], [6], [7]. The former is characterized by its complexity, whereas the latter performs poorly in comparison [2], [3]. Recent research has focused on using machine learning (ML) algorithms in ASI using synthetic signals [8], [9], [10], [11], [12], [13], [14], [15], [16]. ML classification models demonstrated a more robust response to various channel variations than likelihood-based and feature-based classification strategies, when trained with representative and diverse data.

In earlier works, real measurements were used to demonstrate the capability of ML techniques for signal identification [17], [18], including convolutional and feedforward neural networks (NNs). They were used to classify real power spectral density (PSD) measurements into their corresponding cellular signals type. Despite the fact that ML is more computationally efficient than classic ASI techniques, ML algorithms continue to be regarded as resource-intensive [11]. In their training methodology, ML algorithms heavily rely on numerical optimization and backpropagation [19]. In order to compute the error gradient for each NN parameter, these methods necessitate lengthy training periods and costly hardware [19].

Random vector functional link (RVFL) networks were introduced and explained in [20] and [21]. In the earlier times, RVFL was ambitious with regard to hardware capability. Recently, with the advancement of hardware, it was further developed and evaluated in [22] and [23]. Using a single hidden layer and direct connections between the input and output layers, the feedforward network RVFL bypasses the hidden layer. The differentiating feature of the RVFL is that the hidden layer's weights are set randomly and not optimized. Hence, the weights of the output layer are the sole trainable parameters. As a special instance of the RVFL NN, Huang et al. [24] proposed an extreme learning machine (ELM). ELM is an ML algorithm that belongs to the family of single-hidden layer feedforward NNs. It was introduced as a fast and efficient learning algorithm. In ELM, the direct input–output link is disabled [25]. ELM shares the same architecture as conventional feedforward NNs with a single hidden layer. The distinction between them is their respective training methods [26], [27]. Unlike traditional NNs that require iterative training, the ELM adopts a random initialization of the input-to-hidden layer weights and analytically determines the output weights. This approach allows the ELM to achieve fast training speed while maintaining good generalization performance. The ELM can be considered a linear algorithm, gaining nonlinearity from the activation function. ELM has

Esraa A. Makled is with the American University in Cairo, Cairo, Egypt (e-mail: esraa.makled@aucegypt.edu).

Ibrahim Al-Nahhal is with the Faculty of Engineering and Applied Science, Memorial University, St. Johns, NL A1C 5S7, Canada (e-mail: ioalnahhal@mun.ca).

Octavia A. Dobre is with the Faculty of Engineering and Applied Science, Memorial University, St. Johns, NL A1C 5S7, Canada, and also with the Department of Electronic Engineering, Kyung Hee University, Yongin 17104, Republic of Korea (e-mail: odobre@mun.ca).

Oktay Üreten is with Allen–Vanguard Corporation, Ottawa, ON K1G 5B4, Canada (e-mail: oktay.ureten@allenvanguard.com).

Hyundong Shin is with the Department of Electronics and Information Convergence Engineering, Kyung Hee University, Yongin 17104, Gyeonggi, Republic of Korea (e-mail: hshin@khu.ac.kr).

gained popularity in various applications due to its simplicity, computational efficiency, excellent generalization performance at an incredibly rapid learning rate, and ability to handle large-scale datasets [24], [26], [27].

Cellular drive test scanners automatically identify network signals transmitted from base stations by demodulating/decoding radio frequency (RF) signals. The need for detection across multiple channels in a broad spectrum results in a high latency. In this article, the use of ELM shape-based networks is proposed to identify cellular signals belonging to various radio access technologies, namely the universal mobile telecommunications service (UMTS), global system for mobile communications (GSM), and the long-term evolution (LTE) system, using PSD measurements only. Cellular radio access technology networks have been used to trigger radio-controlled improvised explosive devices in many conflict zones around the world. Electronic counter measures techniques against these threats can be more effective if the threat type is identified and appropriate measures are applied in real time. An identification system that relies on PSD measurements only provides a lower latency solution compared to the ones that require decoding information from the cellular network. According to the knowledge of the authors, this is the first proposal of an ELM framework to identify real cellular signal PSD measurements that can be readily applied to real systems. This article offers the following contributions[1] [28].

1) Propose an ELM model to identify over-the-air PSD measurements automatically in real systems, specifically the GSM, UMTS, and LTE cellular signal types.
2) Derive and analyze the training and computational complexities associated with the proposed ELM model that includes training time, number of real multiplications, additions, and parameters necessary for the identification of cellular signals.
3) Assess the robustness of the proposed ELM model against the change in datasets by utilizing two different datasets collected under different conditions.
4) Compare the proposed ELM model against existing literature in terms of its complexity and identification accuracy.

The manuscript is divided as follows. Section II explains the proposed ELM and the system model, Section III shows the computational complexity analysis, Section IV discusses the experimental setup and numerical results, and Section V concludes the work.

II. Proposed Signal Identification Model

A. Model Description of ELM Model

The proposed ELM identification model is depicted in Fig. 1, and consists of three major stages: 1) measurement acquisition; 2) preprocessing; and 3) ELM network processing. In the sections that follow, we provide a detailed explanation of each stage.

[1]These contributions are part of the thesis dissertation of the first author, available at https://research.library.mun.ca/16511/1/Thesis.pdf.

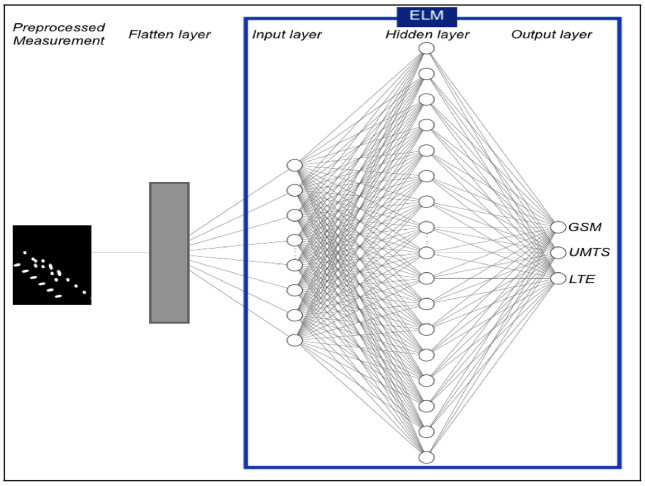

Fig. 1. Proposed ELM identification model.

B. Measurement Acquisition

Over-the-air PSD measurements are gathered from various frequency bands. The PSD measurements belong to GSM, UMTS, and LTE signals. GSM, works at 900 and 1800 MHz frequencies in Europe, and 850 and 1900 MHz in the Americas. UMTS provides higher data rates within the 700–2600 MHz spectrum, while LTE has much higher data transmission rates within quite several bands: 700, 1800, 1900, 2100, and 2600 MHz. Specifically, the PSD value in decibels (dB) at a given frequency bin f is denoted as m_f, where $m_f \in \mathbf{M}$. The vector $\mathbf{M}$ encompasses a single PSD measurement and is expressed as $\mathbf{M} = \{m_1, m_2, \ldots, m_F\}$, where F signifies the total count of frequency bins within a single measurement. The dataset is collected separately from each frequency band to train and test the NN identification model tailored to that band. The construction of each model relies on PSD measurements from the respective frequency band. This approach develops a unique ELM network for each frequency band, with distinct weights and biases.

Fig. 2 provides an illustrative excerpt from the 2100 MHz frequency band dataset. This graphical representation showcases distinct measurements acquired in the 2100 MHz band, which are samples from the larger collection of PSD measurements used to train and test the proposed ELM model tailored for that band.

C. PSD/2-D Image Mapper

In this stage, an image is generated from each measured PSD using the following formula:

$$\mathcal{I} = \left[p_{ab}\right]_{I_H \times I_W} \tag{1}$$

where I_H represents the image height, I_W denotes the image width, and p_{ab} signifies the value assigned to the pixel located at coordinates (a, b) within the image $\mathcal{I}$. Since $\mathcal{I}$ is a 2-D binary image, each p_{ab} assumes a binary state, either 1 or 0, based on the following criterion:

$$p_{ab} = \begin{cases} 1, \text{ if } b = \left\lfloor \frac{I_H(m_a - \phi)}{\Phi - \phi} \right\rceil, & 1 \le a \le I_W. \\ 0, \text{ otherwise} \end{cases} \tag{2}$$

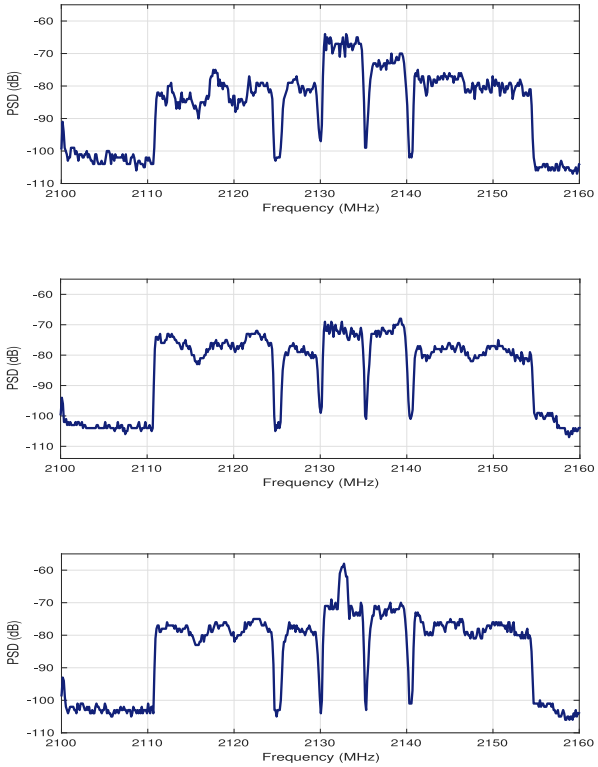

Fig. 2. PSD samples collected from 2100 MHz band.

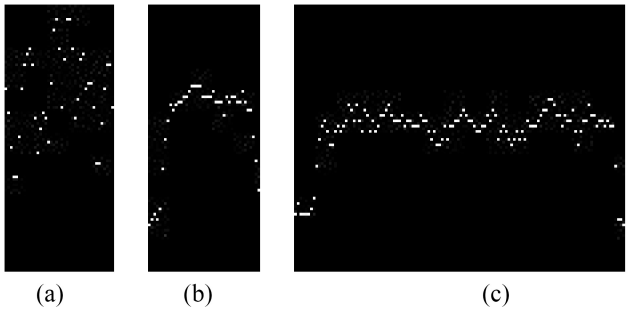

Fig. 3. Samples of I_s. (a) GSM. (b) UMTS. (c) LTE.

In this context, m_a represents the PSD value at bin a, while Φ and ϕ denote the maximum and minimum measurements of the PSD, respectively. These are mathematically expressed as $\Phi = \max_{1\leq a\leq I_W}\{m_a\}$ and $\phi = \min_{1\leq a\leq I_W}\{m_a\}$. I_H is set to 100, and I_W is assigned the value F for all PSDs. All fractional numbers are rounded to the nearest integer value using the $\lfloor\cdot\rceil$ function. By applying this process to each PSD measurement within the acquired dataset, an image is systematically derived to represent each individual PSD measurement comprehensively.

D. Data Preprocessing

In this section, we explain the process of extracting signal images from PSD measurement images. Let S denote the number of signals occupying a single PSD measurement. Consequently, from each PSD measurement, S distinct images are extracted, each representing one of the S signals. We define each signal image, denoted by $\mathcal{I}_s$, as follows:

$$\mathcal{I}_s = \left[p_{ac}\right]_{I_{sH}\times I_{sW}} \forall s = 1, .., S. \tag{3}$$

Here, I_{sH} is selected to be equal to I_H, implying that the full image height is extracted from image $\mathcal{I}$, and I_{sW} represents the horizontal span of the desired signal. In this work, the horizontal span is determined based on automatic channel detection decisions provided by the R&S ROMES software [29].

Each PSD measurement is transformed into S labeled 2-D binary (black and white) images, depicting discrete PSD measurements of individual cellular signals and corresponding labels. A sample of these input 2-D binary images is depicted in Fig. 3. All these images from all PSDs are then gathered for input to the proposed ELM network. All the input 2-D images need to have a standard height and width; this resizing process involves upscaling or downscaling the dimensions of I_{sW} and I_{sH} using bi-cubic interpolation. Since the dimensions of the input images substantially affect the computational complexity and classification accuracy of the proposed ELM model, they are amongst the finely tuned hyperparameters. It is essential to emphasize that because it is implausible to assume prior knowledge of spectrum allocation for ad-hoc deployments, the proposed ELM model does not use the occupied frequency bins and bandwidths as input data.

E. Architecture of ELM

ELM employs randomly assigned weights in the hidden layer and utilizes a linear regression-based method for training the output layer, in contrast to the stochastic gradient descent approach used in traditional neural networks. This section elaborates on the architectural design of ELMs, highlighting their simplicity, rapid convergence, and efficient learning process.

1) Input Layer: The input layer receives data as a feature vector, $\mathbf{x}$. The vector dimensionality, k, represents the number of features characterizing the input data. The input layer preprocesses and normalizes the data to prepare it for further processing [26], [27].

2) Hidden Layer: The distinct feature of ELM is the central layer, where most of the computation takes place [19], [24], [27]. It consists of one layer of hidden neurons with randomly assigned weights and biases. The weight matrix, $\mathbf{W}$, links the input layer to these neurons, and the output, $\mathbf{H}$, is determined by applying an activation function, σ, to the weighted input plus the biases, ζ [27]

$$\mathbf{H} = \sigma(\mathbf{x}\mathbf{W} + \zeta). \tag{4}$$

It identifies complex data patterns with greater efficiency.

3) Output Layer: This layer predicts the output based on the information processed in the hidden layer [26]. The output layer's weights are fine tuned during training, unlike the hidden layer. The output, $\mathbf{O}$, is calculated as $\mathbf{O} = \mathbf{H}\gamma$, where γ represents the weights connecting the hidden and output layers, which are adjusted during training to improve accuracy by minimizing errors [26].

4) Training and Weight Calculation: ELMs randomly assign weights between the input and hidden layers, bypassing the iterative fine-tuning process [27]. This random weight assignment accelerates learning and enhances convergence, reducing the computational complexity typically involved.

However, learning still occurs in the output layer, where the optimal weights γ are determined. ELMs use linear regression to minimize the difference between the predicted outputs $\mathbf{O}$ and the target outputs $\mathbf{Y}$ [26], [27]. The output weights are calculated as $\gamma = \mathbf{H}^{\dagger}\mathbf{Y}$, where $\mathbf{H}^{\dagger}$ is the pseudoinverse of the hidden layer matrix, offering a least-squares solution without the need for backpropagation [25], [27]. ELM's distinctive approach to machine learning comes with its own set of advantages, including rapid training process, efficiency, simplicity, generalization, and robustness [25], [27].

III. Computational Complexity Analysis of the Proposed ELM

In the realm of ML, a fundamental aspect of assessing the suitability of a model for practical applications is understanding its computational complexity. This evaluation provides insights into the computational demands, resource requirements, and efficiency of the model. In the case of the proposed ELM, the computational complexity is assessed by examining parameters, such as the number of weights and biases C_P, the total number of real multiplications C_M, and the overall number of real additions C_A.

A. Parameter Complexity (C_P)

The parameter complexity, denoted as C_P, considers the total number of weights and biases involved in the ELM network. These weights and biases are crucial elements of the NN complexity as they determine the ability of the model to capture and represent complex relationships within the dataset. In the proposed ELM, C_P can be given as

$$C_P = \sum_{i=1}^{N} (\eta_i + 1)\eta_{i+1} \tag{5}$$

where η_i represents the number of neurons in the ith layer of the ELM network. The term $(\eta_i + 1)\eta_{i+1}$ signifies the product of the number of neurons in layers i and $i+1$. The summation extends over all layers of the ELM, including the input and output layers. In the context of an ELM model, the value of N is equal to 3.

B. Real Multiplication Complexity (C_M)

The multiplication count, represented as C_M, quantifies the total number of real multiplications carried out during the execution of the ELM network. Multiplications are computationally expensive operations, and their count is an essential factor in assessing the computing time complexity of the model. To compute C_M, a similar principle is applied as in C_P as

$$C_M = \sum_{i=1}^{N} \eta_i \eta_{i+1}. \tag{6}$$

C. Real Addition Complexity (C_A)

The addition complexity, denoted as C_A, provides insights into the total number of real additions performed in the ELM network. While additions are generally less computationally intensive than multiplications, they still contribute to the overall time complexity of the proposed ELM model. The formula for C_A encompasses two components: first, it includes the sum of products of the number of neurons in each layer i and the number of neurons in the subsequent layer $i + 1$. Second, it accounts for the sum of neurons in the subsequent layer $i + 1$. Thus, C_A can be given as

$$C_A = \sum_{i=1}^{N} \eta_i \eta_{i+1} + \sum_{i=1}^{N} \eta_{i+1}. \tag{7}$$

The complexity metrics (i.e., C_P, C_M, and C_A) offer a comprehensive evaluation of the computational demands and efficiency of the proposed ELM model. C_P provides insights into the memory requirements, while C_M and C_A reflect the computational time and hardware cost for the NN operations.

IV. Experimental Setup and Numerical Results

In this section, the designated hyperparameters of the proposed ELM model are presented, accompanied by an examination of the impact of varying the neurons within the proposed ELM model on identification accuracy. The evaluation of the proposed ELM model is conducted with respect to the identification accuracy on the two datasets, referred to as DS1 and DS2. Additionally, the efficacy of the ELM model is substantiated through a comparative analysis with the most accurate findings in the existing literature.

A. Experimental Setup

We employed a proprietary software-defined radio receiver to collect over-the-air PSD measurements. This receiver operates in the 20–6000 MHz region and can pick up RF signals with a spur-free dynamic range of 70 dB and a noise figure of 10 dB. Hundred MHz is the instantaneous capture bandwidth. The SNR range of the captured data is 10 dB to 50 dB. Prior to being filtered to a 100 MHz bandwidth, the gathered frequency bands undergo band-pass filtering, followed by down-conversion to an intermediate frequency (IF). Each band has its own unique center frequency.

Two separate datasets, DS1 and DS2, each collected at different times, are used to assess the performance of the algorithm. For DS1, the data collection is compiled from four separate bands of frequencies that are used in various regions; these bands are numbered 1 through 4, and their corresponding frequencies are 900, 2100, 1900, and 850 MHz. Band 1 includes 104 PSD signal measurements of GSM and 78 PSD signal measurements of UMTS. Band 2 comprises 1662 PSD signal measurements of UMTS and 2493 PSD signal measurements of LTE. Band 3 encompasses 1652 LTE PSD signal measurements, 1652 PSD signal measurements of UMTS, and 825 PSD signal measurements of GSM. Band 4 includes 2793 PSD signal measurements of UMTS and 2793 PSD signal measurements of GSM. DS2 is available for bands

TABLE I
KEY PARAMETERS USED IN THE ELM MODEL

Parameter	Description
Activation Function	ReLU (Rectified Linear Unit)
Weight Distribution	Beta Distribution with $\alpha = 1$, $\beta = 3$
Input Image Dimensions	100×30 pixels

2–4, with band 2 containing 5696 UMTS PSD signal measurements and 8544 LTE PSD signal measurements, band 3 having 3454 LTE PSD signal measurements, 3454 UMTS PSD signal measurements, and 1727 GSM PSD signal measurements, and band 4 consisting of 2688 UMTS PSD signal measurements and 2688 GSM signal measurements. The acquired PSD signal measurements are utilized to build balanced training and testing datasets with 70% used for training and 30% assigned for testing. Subsequently, collected datasets are exported to American standard code for information interchange (ASCII) files for processing in MATLAB software. The processed PSD measurements are broken down into their individual cellular signals using MATLAB, in accordance with the procedure described in Section II. After that, the images of the signal measurements are sent into a Python code that builds and evaluates the proposed ELM model.

By utilizing the R&S TSME drive test scanner tool and ROMES software with its automated channel detection feature, accurate labels of PSD measurements of cellular signals across various cellular bands can be acquired for further applications in both training and testing scenarios of the proposed ELM model.

B. Proposed ELM Model Hyperparameters

The rectified linear unit (ReLU) activation function, denoted as σ, introduces nonlinearity into the model, thereby enhancing its expressive capabilities. The choice of ReLU was based on its simplicity and compatibility with the beta distribution, which encourages sparse activations for fast training and good generalization in ELM. The selection of the input random distribution contributes to the model's ability to capture intricate data patterns and relationships effectively. In the proposed ELM model, a beta distribution with $\alpha = 1$ and $\beta = 3$ is chosen to initialize the weights and biases within the network. The beta distribution was selected based on empirical analysis showing this choice to be effective in weight initialization, as the model converged faster during training compared to other distributions and parameter settings. The dimensions of the input images are adjusted to be 100 by 30 pixels. These dimensions were chosen based on extensive experimentation to achieve a tradeoff between complexity and performance. Table I shows the parameters of the ELM model. It is noteworthy that the hyperparameters of the proposed ELM are exclusively optimized using the DS1 dataset. Subsequently, the DS2 dataset is employed to assess the generalization and robustness of the proposed ELM model under the conditions where the hyperparameters have been optimized using DS1.

The determination of the number of hidden neurons holds a pivotal role in shaping the capacity and learning capability of the ELM model. Treated as a hyperparameter, the number of hidden nodes undergoes meticulous tuning, allowing for the optimization of the overall performance of the ELM network. This tuning process aims to strike a balance between the model complexity and the acquisition of generalization abilities. A detailed discussion on tuning the number of hidden neurons is presented in the following section.

C. Optimizing Hidden Neurons of the Proposed ELM Model

In this section, a systematic variation of the number of hidden neurons was executed to optimize the performance (i.e., the identification accuracy and computational complexity) of the proposed ELM model across different frequency bands within DS1.

Fig. 4 depicts the relation between the number of hidden neurons and the identification accuracy for each frequency band. Notably, for band 1, the identification accuracy reached 100% across all cellular signal types with the utilization of 500 hidden neurons. Regarding bands 2 and 3, the accuracy approached 100% when the number of hidden neurons reached approximately 4000, although satisfactory accuracy levels were maintained at around 1000 hidden neurons for both bands. Band 4 demonstrated stability at 1000 hidden neurons. In the proposed ELM model, a nuanced selection of 1130 hidden neurons was made through meticulous fine-tuning, aiming to achieve optimal accuracy with minimal complexity, considering the increment in the number of neurons.

D. Assessing the Proposed ELM Model Using DS1: Hyperparameters' Selection Assessment

Table II presents a comprehensive overview of the experimental findings derived from the DS1 dataset using the proposed ELM model with hyperparameters optimized based on DS1. The table offers detailed insights into the average identification accuracy percentages for UMTS, GSM, and LTE cellular signals. The proposed ELM model attains an identification accuracy of 100% for bands 1 and 4. Bands 2 and 3 consistently exhibit near-perfect identification accuracy percentages, consistently surpassing 99.2%. The proposed ELM model demonstrates exceptional accuracy, achieving 99.9%, 99.7%, and 99.6% identification accuracy for GSM, UMTS, and LTE, respectively. The outcomes obtained from the proposed ELM model underscore its efficacy in discerning various cellular communication technologies.

To visualize the proposed ELM model's performance, Fig. 5 presents the confusion matrices across all frequency bands. A confusion matrix succinctly evaluates the accuracy and error characteristics of a classification model by quantifying true positives, true negatives, false positives, and false negatives. It serves as a pivotal tool for assessing the proficiency of the proposed model in distinguishing distinct classes within a dataset. The results indicate that the proposed ELM model achieves a perfect confusion matrix with negligible occurrences of false negatives and false

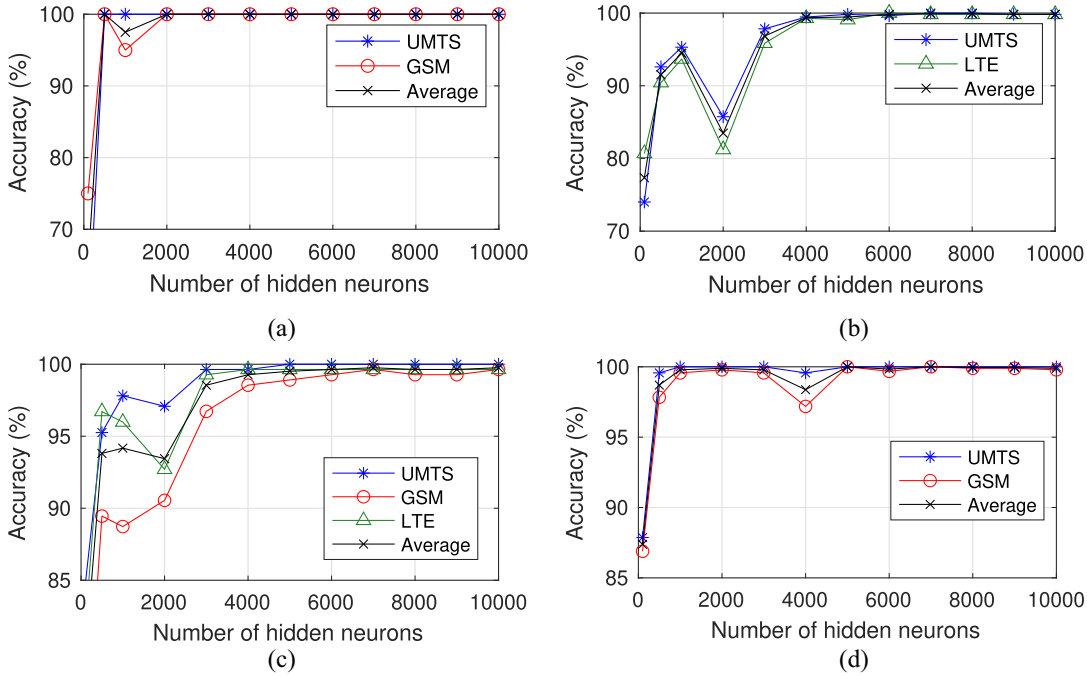

Fig. 4. Effect of varying the number of hidden neurons in DS1 on: (a) band 1, (b) band 2, (c) band 3, and (d) band 4.

TABLE II
IDENTIFICATION ACCURACY OF THE PROPOSED ELM MODEL DS1

Band	Accuracy UMTS	Accuracy GSM	Accuracy LTE	Avg. accuracy
1	100%	100%	-	100%
2	99.7%	-	99.4%	99.6%
3	99.2%	99.6%	99.8%	99.6%
4	100%	100%	-	100%

positives, accurately identifying all true positives and true negatives.

E. Assessing the Proposed ELM Model Using DS2: Generalization and Robustness Assessment

To further assess the generality and robustness of the proposed ELM model, we applied the same model, without retuning, to an unseen DS2 dataset. It is crucial to emphasize that the DS1 and DS2 datasets were obtained under distinct conditions, as mentioned previously. The identification accuracy results are summarized in Table III. Remarkably, when the dataset was utilized in conjunction with the generalized ELM model structure, all cellular technologies achieved an average identification accuracy exceeding of 92%. The minimum identification accuracy achieved is 90.1% for UMTS in band 3.

Fig. 6 displays the confusion matrix of the proposed ELM model for DS2. The confusion matrix reveals that GSM is never confused with LTE, and vice versa. Furthermore, it indicates that any confusion that occurs is minimal, despite the proposed ELM model not being trained on this dataset at all. This outcome underscores the model's capability to maintain high identification accuracy even in situations where stationary data collection is not feasible, and fine tuning the proposed ELM model for specific scenarios is not a possibility. These results demonstrate the robustness and practical applicability of the proposed ELM algorithm in real-world wireless communication systems.

F. Assessing the Proposed ELM Model Compared to Literature

In the existing literature, a hybrid convolutional feedforward neural network (HCFNN) model was introduced in [18], as a solution for identifying GSM, UMTS, and LTE cellular signals from images. The HCFNN model represents a hybrid architecture incorporating multiple convolutional layers and a feedforward neural network. Maxpooling and dropout techniques are also applied within the network. The identification accuracy of the HCFNN model was benchmarked against several earlier works in the literature, including [6] and [17]. The HCFNN model demonstrated its superiority over other proposed models in the literature. In this section, we conduct a comparative analysis of the performance of the proposed ELM model with the HCFNN model [18], reported as one of the most efficient and accurate models in the literature.

Fig. 7(a) visually illustrates the comparison of identification accuracy between the proposed ELM model and the HCFNN model in [18], focusing on the accuracy of identifying cellular PSD measurements in the DS1 dataset. This figure demonstrates that the proposed ELM model consistently achieves superior identification accuracy across different cellular technologies. Specifically, the proposed ELM outperforms

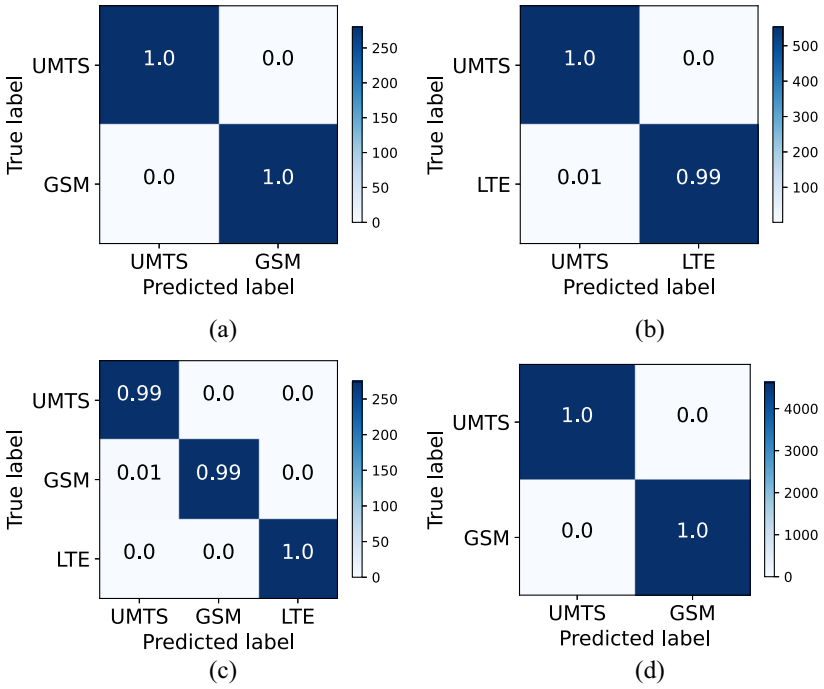

Fig. 5. Normalized confusion matrices for different bands in DS1. (a) Band 1. (b) Band 2. (c) Band 3. (d) Band 4.

TABLE III
IDENTIFICATION ACCURACY ELM FOR DS2

Band	Accuracy UMTS	Accuracy GSM	Accuracy LTE	Avg. accuracy
2	96.6%	-	96.3%	96.5%
3	90.1%	90.9%	97.4%	92.8%
4	98.8%	91.1%	-	94.9%

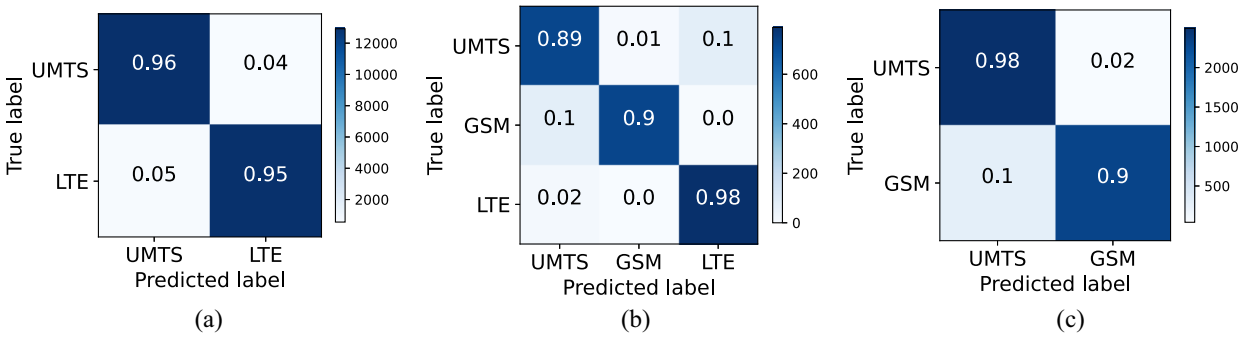

Fig. 6. Normalized confusion matrices for different bands in DS2. (a) Band 2. (b) Band 3. (c) Band 4.

HCFNN with an improvement in the identification accuracy of 3%, 2%, and 1% for UMTS, GSM, and LTE, respectively, resulting in an average accuracy improvement of 2%. Fig. 7(b) further reveals that the HCFNN model encounters challenges when identifying cellular technologies with the unseen dataset of DS2. In this context, the proposed ELM model's accuracy improvement over the HCFNN model increases to 8%, 1%, and 3% for UMTS, GSM, and LTE, respectively, providing an average accuracy improvement of 4%. In conclusion, Fig. 7 highlights that the proposed ELM model not only exhibits better identification accuracy compared to the most efficient model in the literature but also demonstrates enhanced robustness and generalization capabilities for unseen datasets.

The comparison of the complexity between the proposed ELM model and the HCFNN model in [18], is presented in Fig. 8. The complexity assessment is divided into two components: 1) the time complexity consumed in the training phase (i.e., the time to learn the neural network model) and 2) the complexity cost for the testing phase [i.e., C_P, C_M, and C_A as in (5)–(7)]. As depicted in Fig. 8(a), the training time complexity of the proposed ELM is 7.5 times less than the training complexity of the HCFNN. For the testing complexity cost, the proposed ELM model exhibits similar values to HCFNN for C_M and C_A, but it shows a higher number of required parameters, C_P, as shown in Fig. 8(b).

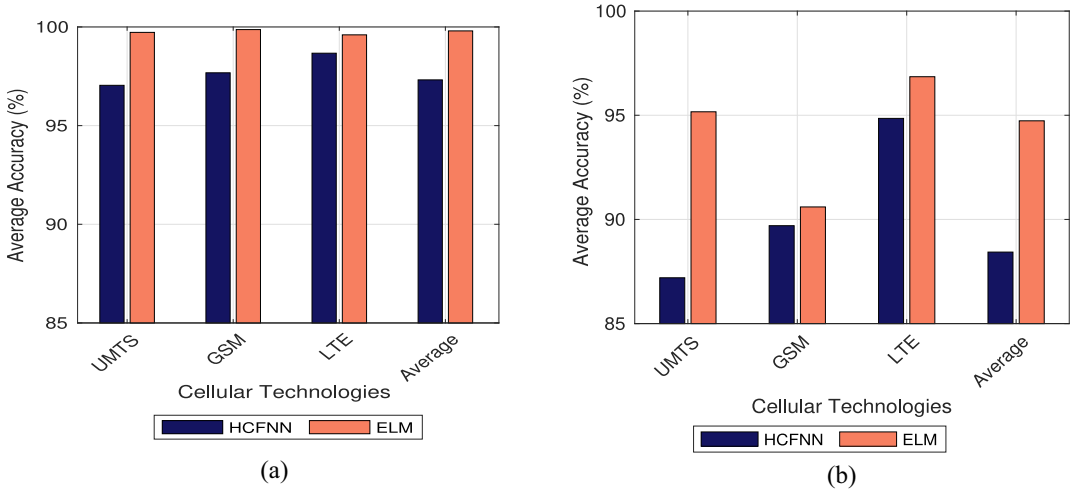

Fig. 7. Comparison between identification accuracy of the proposed ELM model and HCFNN [18]. (a) DS1. (b) DS2.

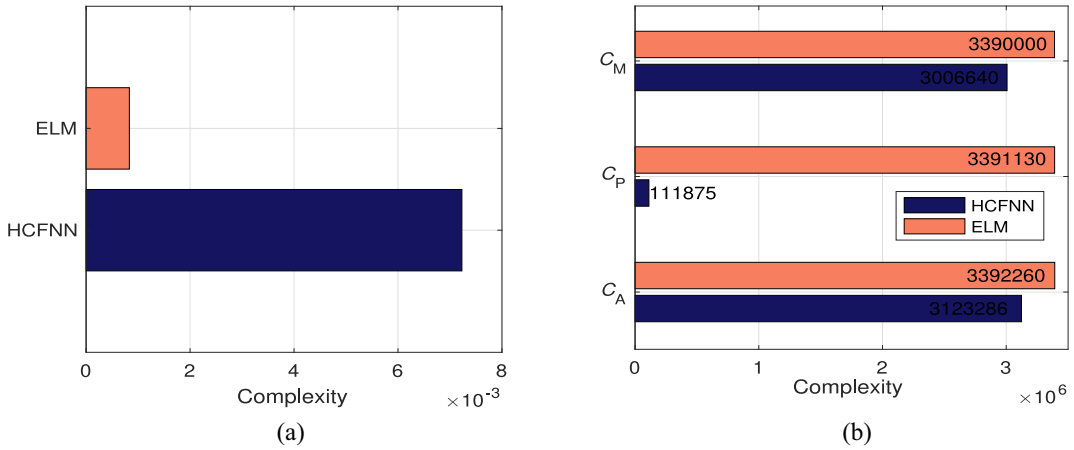

Fig. 8. Complexity comparison between the proposed ELM model and HCFNN [18]. (a) Training time complexity. (b) Testing complexity cost.

In light of this comparative analysis, it becomes evident that the proposed ELM model consistently outperforms the HCFNN model across different situations, offering superior identification accuracy and significantly reduced training time, albeit with a slight increase in the number of stored parameters required for testing.

V. Conclusion

In response to the escalating demand for efficient spectrum utilization due to the proliferation of wireless devices, this study proposes an ELM model for the identification of real PSD measurements in cellular systems, including LTE, UMTS, and GSM. The hyperparameters of the ELM model are rigorously optimized using the DS1 dataset, while the unexplored DS2 dataset is employed to assess the model's robustness and generality. An evaluation based on the derived complexity cost and experimental results demonstrates the proposed ELM model's remarkable performance, achieving nearly 100% identification accuracy for all cellular signal types. Additionally, the proposed ELM model undergoes a comparative analysis with the most efficient model in the literature, namely the HCFNN model. This comparison encompasses both the DS1 and DS2 datasets, with DS1 contributing to the model's development and DS2 representing an unseen dataset. Remarkably, the proposed ELM model, with a training time complexity 7.5 times less than the HCFNN model, exhibits notable superiority across all cellular technologies, yielding an improvement in the identification accuracy ranging from 1% to 8%. As a future research, more sophisticated ELM techniques will be investigated, and the approach proposed may be further generalized to include 5G technology.

References

[1] Y. A. Eldemerdash, O. A. Dobre, O. Üreten, and T. Yensen, "Identification of cellular networks for intelligent radio measurements," *IEEE Trans. Instrum. Meas.*, vol. 66, no. 8, pp. 2204–2211, Aug. 2017.

[2] Y. A. Eldemerdash, O. A. Dobre, O. Üreten, and T. Yensen, "Fast and robust identification of GSM and LTE signals," in *Proc. IEEE Int. Instrum. Meas. Technol. Conf.*, 2017, pp. 1–6.

[3] F. Hameed, O. A. Dobre, and D. C. Popescu, "On the likelihood-based approach to modulation classification," *IEEE Trans. Wireless Commun.*, vol. 8, no. 12, pp. 5884–5892, Dec. 2009.

[4] E. Karami, O. A. Dobre, and N. Adnani, "Identification of GSM and LTE signals using their second-order cyclostationarity," in *Proc. IEEE Int. Instrum. Meas. Technol. Conf.*, 2015, pp. 1108–1112.

[5] O. A. Dobre, "Signal identification for emerging intelligent radios: Classical problems and new challenges," *IEEE Instrum. Meas. Mag.*, vol. 18, no. 2, pp. 11–18, Apr. 2015.

[6] E. A. Makled, A. A. Al-Habob, O. A. Dobre, and O. Üreten, "Detection and identification of mobile network signals," *IEEE Trans. Instrum. Meas.*, vol. 70, pp. 1–4, Sep. 2021.

[7] D. Grimaldi, S. Rapuano, and L. De Vito, "An automatic digital modulation classifier for measurement on telecommunication networks," *IEEE Trans. Instrum. Meas.*, vol. 56, no. 5, pp. 1711–1720, Oct. 2007.

[8] H. Agirman-Tosun et al., "Modulation classification of MIMO-OFDM signals by independent component analysis and support vector machines," in *Proc. Conf. Rec. 45th Asilomar Conf. Signals, Syst. Comput.*, 2011, pp. 1903–1907.

[9] F. Xing, D. Xu, W. Xu, and H. Wang, "A modulation recognition algorithm of communication signals and implementation based on digital signal processor," in *Proc. IEEE MTT-S Int. Wireless Symp.*, 2021, pp. 1–3.

[10] M. D. Wong, S. K. Ting, and A. K. Nandi, "Naive Bayes classification of adaptive broadband wireless modulation schemes with higher order cumulants," in *Proc. 2nd Int. Conf. Signal Process. Commun. Syst.*, 2008, pp. 1–5.

[11] X. Li, F. Dong, S. Zhang, and W. Guo, "A survey on deep learning techniques in wireless signal recognition," *Wireless Commun. Mobile Comput.*, vol. 2019, pp. 1–12, Feb. 2019.

[12] H. Xia et al., "Cellular signal identification using convolutional neural networks: AWGN and rayleigh fading channels," in *Proc. IEEE Int. Symp. Dyn. Spectrum Access Netw.*, 2019, pp. 1–5.

[13] M. L. D. Wong and A. K. Nandi, "Automatic digital modulation recognition using spectral and statistical features with multilayer perceptrons," in *Proc. 6th Int. Symp. Signal Process. Appl.*, vol. 2, 2001, pp. 390–393.

[14] A. K. Nandi and E. E. Azzouz, "Algorithms for automatic modulation recognition of communication signals," *IEEE Trans. Commun.*, vol. 46, no. 4, pp. 431–436, Apr. 1998.

[15] J. A. Snoap, D. C. Popescu, and C. M. Spooner, "Deep-learning-based classifier with custom feature-extraction layers for digitally modulated signals," *IEEE Trans. Broadcast.*, vol. 70, no. 3, pp. 763–773, Sep. 2024.

[16] J. A. Snoap, D. C. Popescu, J. A. Latshaw, and C. M. Spooner, "Deep-learning-based classification of digitally modulated signals using capsule networks and cyclic cumulants," *Sensors*, vol. 23, no. 12, p. 5735, 2023.

[17] E. A. Makled, I. Al-Nahhal, O. A. Dobre, and O. Üreten, "Identification of cellular signal measurements using machine learning," *IEEE Trans. Instrum. Meas.*, vol. 72, pp. 1–4, Jan. 2023.

[18] E. A. Makled, I. Al-Nahhal, O. A. Dobre, O. Üreten, and H. Shin, "Identification of cellular measurements: A neural network approach," *IEEE Trans. Instrum. Meas.*, vol. 73, pp. 1–12, Oct. 2023.

[19] U. Markowska-Kaczmar and M. Kosturek, "Extreme learning machine versus classical feedforward network," *Neural Comput. Appl.*, vol. 33, no. 22, pp. 15121–15144, 2021.

[20] Y.-H. Pao, S. M. Phillips, and D. J. Sobajic, "Neural-net computing and the intelligent control of systems," *Int. J. Control*, vol. 56, no. 2, pp. 263–289, 1992.

[21] Y.-H. Pao, G.-H. Park, and D. J. Sobajic, "Learning and generalization characteristics of the random vector functional-link net," *Neurocomputing*, vol. 6, no. 2, pp. 163–180, 1994.

[22] M. Ganaie, M. Tanveer, and P. N. Suganthan, "Minimum variance embedded random vector functional link network," in *Proc. Int. Conf. Neural Inf. Process.*, Nov. 2020, pp. 412–419.

[23] L. Zhang and P. N. Suganthan, "A comprehensive evaluation of random vector functional link networks," *Inf. Sci.*, vols. 367–368, pp. 1094–1105, Nov. 2016.

[24] G.-B. Huang, Q.-Y. Zhu, and C.-K. Siew, "Extreme learning machine: A new learning scheme of feedforward neural networks," in *Proc. IEEE Int. Joint Conf. Neural Netw.*, vol. 2, 2004, pp. 985–990.

[25] W. Cao, X. Wang, Z. Ming, and J. Gao, "A review on neural networks with random weights," *Neurocomputing*, vol. 275, pp. 278–287, Jan. 2018.

[26] G.-B. Huang, H. Zhou, X. Ding, and R. Zhang, "Extreme learning machine for regression and multiclass classification," *IEEE Trans. Syst., Man, Cybern., B, (Cybern)*, vol. 42, no. 2, pp. 513–529, Apr. 2012.

[27] G.-B. Huang, Q.-Y. Zhu, and C.-K. Siew, "Extreme learning machine: Theory and applications," *Neurocomputing*, vol. 70, nos. 1–3, pp. 489–501, 2006.

[28] E. A. Makled, "Advanced optimization and machine learning techniques for efficient wireless communication networks," Ph.D. dissertation, Faculty Eng. Appl. Sci., Memorial Univ., St. John's, NL, Canada, 2024.

[29] *R&S® ROMES4 Drive Test Software*, Rohde Schwartz, Munich, Germany, Apr. 2021.